Constrained Belief Updates Explain Geometric Structures in Transformer Representations

Mateusz Piotrowski,[1] Paul M. Riechers,[2, 3, *] Daniel Filan,[1] and Adam S. Shai[2, †]

[1] *MATS, Berkeley, CA*
[2] *Simplex, Astera Institute, Emeryville, CA*
[3] *Beyond Institute for Theoretical Science (BITS), San Francisco, CA*

(Dated: February 5, 2025)

What computational structures emerge in transformers trained on next-token prediction? In this work, we provide evidence that transformers implement constrained Bayesian belief updating—a parallelized version of partial Bayesian inference shaped by architectural constraints. To do this, we integrate the model-agnostic theory of optimal prediction with mechanistic interpretability to analyze transformers trained on a tractable family of hidden Markov models that generate rich geometric patterns in neural activations. We find that attention heads carry out an algorithm with a natural interpretation in the probability simplex, and create representations with distinctive geometric structure. We show how both the algorithmic behavior and the underlying geometry of these representations can be theoretically predicted in detail—including the attention pattern, OV-vectors, and embedding vectors—by modifying the equations for optimal future token predictions to account for the architectural constraints of attention. Our approach provides a principled lens on how gradient descent resolves the tension between optimal prediction and architectural design.

I. INTRODUCTION

Transformers excel at next-token prediction [22], but their success belies a fundamental tension: optimal prediction requires Bayesian belief updating—a recursive process—while their architecture enforces parallelized, attention-driven computation. How do transformers resolve this conflict? We show that they develop geometrically structured representations that approximate Bayesian inference under architectural constraints, revealing a precise interplay between theoretical necessity and implemented solution.

In this work, we combine insights from the theory of optimal prediction with neural network analysis. First, computational mechanics [12, 15, 17–19] dictates *what* an optimal predictor must represent: belief states that encode distributions over futures. Second, mechanistic interpretability reveals *how* transformers approximate these states under architectural constraints, bending Bayesian updates into attention's parallelizable form [6, 13].

By combining these frameworks we reveal *why* transformers learn certain intermediate structures. We find that the geometry of a transformer's internal representations is not an accident—it is a mathematical signature of how architectural constraints warp otherwise optimal Bayesian inference. By interpreting learned weights and activations via standard mechanistic interpretability, we uncover an algorithm that is well-captured by the **constrained belief updating** equations. From first principles, we derive the constrained belief geometries, and reverse-engineer the transformer's computational blueprint, predicting attention patterns, value vectors, and residual stream geometries precisely. Thus, beyond verifying that transformers encode belief states, we show how the specific circuits that implement those states necessarily deviate from the unconstrained Bayesian ideal in predictable and theoretically tractable ways.

To concretize these ideas, we focus on transformers trained on data from the Mess3 class of hidden Markov models (HMMs) [12], which provides rich and visualizable belief-state geometries and also admits a tractable optimal predictor. This allows us to rigorously compare the theoretically optimal geometry with the neural-activation geometry that transformers learn. More broadly, we anticipate that the same tension between architecture and optimal inference arises in large language models trained on natural text, and that our methodology would shed light on those more complex cases.

Key contributions:

1. **A Unified View of Optimal Prediction and Transformer Computation**: We bridge the model-agnostic theory of Bayesian belief states with the model-specific constraints of attention-based parallel processing. This synthesis explains why transformers trained on next-token prediction discover a distinct "constrained belief updating" geometry—balancing optimal Bayesian inference with the functional form of attention.
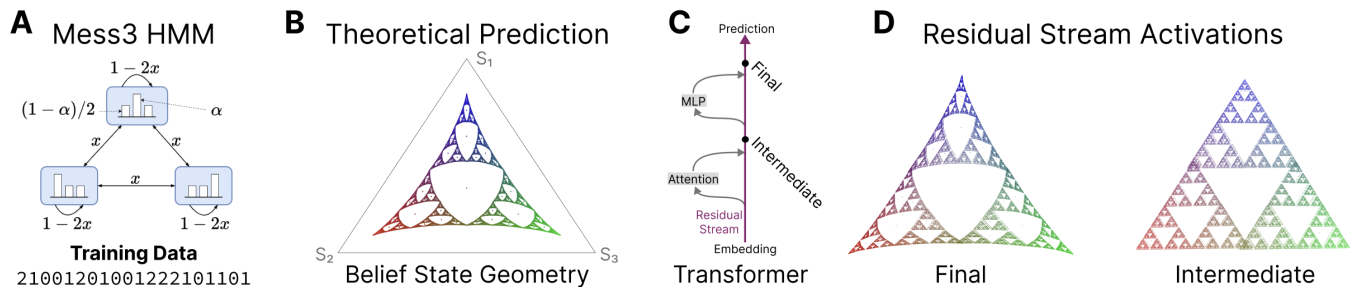
FIG. 1. Transformers' internal representations exhibit complex geometric structure matching the belief-state geometry. **(A)** Mess3 HMM, vertices represent hidden states with their emission distributions. **(B)** Ground-truth belief state geometry of Mess3. Each point represents a belief-state probability distribution over hidden states of the HMM, induced via Bayesian updates upon a sequence of observed emissions, with proximity to the vertices of the simplex corresponding to the probabilities of the three hidden states. **(C)** Schematic of a single-layer transformer with Intermediate activations after Attention, and Final activations after the subsequent MLP. **(D)** PCA projections of the model's final residual stream (left), before the unembedding, reveals a geometric representation that closely matches the belief geometry shown in (B), whereas the PCA projection of the intermediate residual stream (right) after attention but before the MLP exhibits an intricate but different structure. In (B) and (D), points are colored according to the ground-truth belief states associated with the sequence of tokens that induces the point, taking the three constituent probabilities over hidden states of the HMM as RGB values.

2. **Spectral Theory of Constrained Belief Updating**: We develop a theoretical framework that analyzes how eigenvalues of the data-generating transition matrices determine attention heads' behavior. By decomposing belief updates spectrally, we show that multi-head attention naturally implements these scalar updates in orthogonal modes—even handling oscillatory decay of influence—through a sum of specialized head outputs.

3. **Predictive Experiments and Mechanistic Verification**: Our approach yields specific, testable predictions about attention patterns, value vectors, intermediate "fractal" representations, and final belief-state geometry. We confirm these predictions in trained transformers, demonstrating how the inherently recurrent next-token task is realized by an attention-based, parallelized implementation of Bayesian belief updates.

II. BACKGROUND

A. Related Work

In this section we highlight the key connections and distinctions between our approach and prior work, emphasizing how we build upon existing methods while forging a novel path towards understanding the internal mechanisms of transformers. We focus on three main themes: 1) the geometric perspective of neural network representations, particularly the view of features as directions; 2) the circuit-centric framework for mechanistic interpretability;

and 3) the application of computational mechanics and belief state geometry to neural network analysis.

Features as directions in activation space. — Modern interpretability research views neural network representations through the lens of linear geometry, analyzing how activation patterns align with specific directions that encode fundamental features [14]. This perspective is particularly useful given superposition [7], where networks encode more features than available neurons using non-orthogonal vectors. Conceptualizing features as linear directions has been instrumental [1, 5, 20] in understanding what information transformers represent, with geometric relationships between features revealing structured internal representations [8]. Our work complements this line of research by providing a mechanistic explanation for these non-orthogonal geometric structures, providing the theoretical "why" to complement the "what" of feature representations.

From features to circuits. — While feature directions reveal what information is encoded, understanding how networks process this information benefits from identifying computational circuits—subnetworks that implement specific algorithmic operations. These circuits typically combine simpler features into more complex ones as information flows through the network. Notable examples include circuits that detect syntax in language models [6], implement indirect object identification [23], or perform basic arithmetic [13]. However, identifying these circuits remains largely a manual process, starting from observed behaviors and working backwards to discover relevant components (although active research is developing automated approaches; see Conmy et al. [2], Marks et al. [11]).

Our work contributes to this area by demonstrating that a principled, top-down theoretical framework, based on constrained belief updating, can guide the search for circuits and provide a deeper understanding of their function within the larger network. We show how specific circuits in the attention mechanism directly implement the computations predicted by our theory.

Belief state geometry and computational mechanics. — Our work draws inspiration from computational mechanics, a framework for studying the physics of information processing in dynamical systems [4, 17, 19]. When applied to sequential data, computational mechanics, in accordance with the POMDP framework [9], shows that optimal prediction requires maintaining beliefs about the underlying latent states of the data-generating process [21]. These belief states can be visualized as points on a probability simplex, evolving according to Bayesian updating rules, and forming characteristic geometric patterns [3, 12]. Recent work shows that transformer networks naturally discover and encode these belief state geometries in their activation patterns [18]. This connection offers a principled way to analyze network representations: rather than reverse-engineering observed behaviors, we can study how architectural constraints shape the network's implementation of theoretically optimal prediction strategies.

This is the approach taken here. We move beyond prior work by proposing and validating a theory of constrained belief updating, demonstrating how specific architectural elements, like the attention mechanism, modify the idealized belief state dynamics. This perspective shifts the focus from reverse-engineering learned features to understanding why particular geometric patterns emerge during training as a consequence of the interplay between optimal prediction and architectural constraints. Our work provides a concrete example of how this theoretical framework can be applied to understand the internal mechanisms of transformers.

B. Optimal Prediction and Belief State Geometry

Shai et al. [18] showed that transformers minimizing next-token loss must internally represent the context-induced probability density over the entire future of possible token sequences:

$$\Pr(Z_{d+1:}|Z_{1:d} = z_{1:d}) \tag{1}$$

where $Z_{d+1:}$ denotes the sequence of random variables for future tokens, $Z_{1:d}$ denotes the sequence of random variables for past tokens, which is realized by a particular sequence of tokens $z_{1:d} \in \mathcal{Z}^d$ known as the context up to position d.

When we conceptualize the training data as being generated by an edge-emitting hidden Markov model (Mealy HMM), we can derive a natural geometric embedding for these conditional probability distributions. HMMs generate training data by emitting tokens when moving among its hidden states $\mathcal{S}$, from one hidden state S_t at time t to the next. The natural geometric embedding is then given by considering how an initial distribution over hidden states $S_0 \sim \boldsymbol{\eta}_\varnothing$, as a point in the vector space $\mathbb{R}^{|\mathcal{S}|}$ (with coordinates given by the probability elements), evolves upon seeing a particular sequence of tokens, $z_{1:d}$. This distribution over the hidden states, which uniquely induces a probability density over all possible futures, is updated via Bayes rule according to the substochastic transition matrices of the HMM, $\left(T^{(z)}\right)_{z \in \mathcal{Z}}$, with matrix elements $T_{s,s'}^{(z)} = \Pr(Z_{t+1} = z, S_{t+1} = s'|S_t = s)$. In particular, the updated distribution, given context $z_{1:d}$, is the row vector

$$\vec{r}_{\text{full}}^{(z_{1:d})} = \frac{\boldsymbol{\eta}_\varnothing T^{(z_{1:d})}}{\boldsymbol{\eta}_\varnothing T^{(z_{1:d})}\mathbf{1}} \ , \tag{2}$$

where $T^{(z_{1:L})} = T^{(z_1)} \cdots T^{(z_L)}$, and $\mathbf{1}$ is the column vector of all ones. In this paper, we will make the simplifying assumption that the training data is sampled from a stationary stochastic process, in which case the initial distribution over latent states is the stationary distribution $\boldsymbol{\eta}_\varnothing = \boldsymbol{\pi} = \boldsymbol{\pi}T$, where $T = \sum_{z \in \mathcal{Z}} T^{(z)}$ is the row-stochastic transition matrix over hidden states.

Thus, Eq. (2) embeds each token sequence into a probability simplex over the latent states of the HMM—a point in a real-valued vector space. The totality of these points forms a particular geometry, called the belief state geometry, and is universally found in linear form within the activations of various deep neural networks, including RNNs [15] and transformers [18].

This precise framework for anticipating intermediate activations in transformers provides a natural interpretation of the attention mechanism in which it moves information in a belief simplex for the purposes of building up the architecture-independent belief state geometry given in Eq. (2).

III. METHODOLOGY

Data Generation. — Our study focuses on the Mess3 parametrized family of hidden Markov models [12], which provide a tractable yet rich setting for studying sequence prediction. As shown in Fig. 1A, these HMMs consist of

three hidden states with observable emissions controlled by parameter α and transitions by parameter x. Higher values of $\alpha \in [0, 1]$ mean each state more strongly prefers its unique emission symbol, providing clearer information about the generating state. The parameter $x \in (0, \frac{1}{2}]$ controls state persistence—low values create high inertia where states tend to persist, while high values increase transition probabilities between states. For each experimental run, we generate sequences by sampling from an HMM with specific (α, x) values.

Training Process. — We train a standard transformer model on next-token prediction using gradient descent, with sequences sampled from our parametrized HMMs as training data. The model learns to predict the next token in each sequence by minimizing cross-entropy loss (see Appendix B for architecture details).

Analysis of Learned Representations. — To study how the model processes information, we analyze both intermediate and final activations in the residual stream (Fig.1C). We apply principal component analysis (PCA) to these activations across all possible input sequences, finding that the representations are well-captured by a low-dimensional space. In some cases, we slightly rotate the PCA basis to align with theoretically meaningful directions. This dimensionality reduction enables us to visualize how the representations evolve through the network—from the input embeddings, through the intermediate state after attention, to the final output state after the MLP layer (Fig.1D).

Study of Network Computations. — To understand how the network manipulates these representations, we analyze the learned weights and attention patterns. We examine how the attention mechanism transforms input embeddings into intermediate representations, and then study how the MLP layer transforms these intermediate states into the final geometry. At each stage, we compare the learned representations to theoretical predictions derived from optimal Bayesian updates.

IV. RESULTS

A. Intermediate representations are fractals, but not belief state geometry

Through principal component analysis of the residual stream, we observe two distinct fractal structures in transformers trained on Mess3 HMM data: one after the attention mechanism but before the MLP, and another in the final layer output (Figs. 1, 4). While the final representations align with theoretical belief state geometry, the intermediate fractals exhibit a markedly different structure. The systematic difference between intermediate and

final representations raises two key questions: (1) How does the attention mechanism construct these intermediate fractals and (2) why do they take these particular geometric forms? The following results address these questions by revealing the algorithmic process behind their construction and providing a theoretical explanation for their previously unexpected structure.

B. Intermediate representations are built by algorithms in the belief simplex

To determine how the intermediate representation is constructed by the transformer, we performed mechanistic interpretability on the attention heads. We find that attention performs an algorithm with a direct interpretation in the belief simplex.

At every context position, the 'residual stream' can be thought of as the d_{model}-dimensional 'skip connection' communication channel streaming alongside all layers, which carries all working memory in a transformer [6]. Attention and MLP modules read in linear transformations of the residual stream and then add their output to the local residual stream at each layer [22].

Following [6], we decompose the attention operation into two circuits: (i) the output-value (OV) circuit, which specifies what information should be read from each position and how it linearly transforms into a vector that can be broadcast to other positions, and (ii) the query-key (QK) circuit, which compares the similarity of a linearly transformed source and destination to determine how much to update the destination's residual stream with that source's OV contribution.

For a single attention head, the update to the residual stream $\vec{x}_{\mathrm{d}}^{(\mathrm{mid})} = \vec{x}_{\mathrm{d}}^{(\mathrm{pre})} + \vec{c}_{\mathrm{d}} \in \mathbb{R}^{d_{\mathrm{model}}}$ at the *destination* position d is given by:

$$\vec{c}_{\mathrm{d}} = \sum_{\mathrm{s} \leq \mathrm{d}} A_{\mathrm{d,s}} \vec{v}_{\mathrm{s}} \qquad (3)$$

Here, $\vec{v}_{\mathrm{s}} = W_{\mathrm{O}} W_{\mathrm{V}} \vec{x}_{\mathrm{s}}^{(\mathrm{pre})}$ represents the OV circuit's contribution from *source* position s, where W_{O} and W_{V} are the attention output and value weight matrices respectively, and $\vec{x}_{\mathrm{s}}^{(\mathrm{pre})}$ is the incoming residual stream vector at position s. Attention $A_{\mathrm{d,s}}$ is determined by the QK circuit through query–key inner product and the causally masked softmax operations:

$$A_{\mathrm{d,s}} = \delta_{s \leq d} \, \frac{e^{\vec{q}_{\mathrm{d}} \cdot \vec{k}_{\mathrm{s}}/\sqrt{d_{\mathrm{h}}}}}{\sum_{s'=1}^{\mathrm{d}} e^{\vec{q}_{\mathrm{d}} \cdot \vec{k}_{\mathrm{s'}}/\sqrt{d_{\mathrm{h}}}}} \; , \qquad (4)$$

where $\vec{q}_{\mathrm{d}} = W_{\mathrm{Q}} \vec{x}_{\mathrm{d}}^{(\mathrm{pre})}$ is the query vector from destination position d, $\vec{k}_{\mathrm{s}} = W_{\mathrm{K}} \vec{x}_{\mathrm{s}}^{(\mathrm{pre})}$ is the key vector from

A Embedding and OV Vectors

B Theoretical Prediction

C Attention Pattern over All Inputs

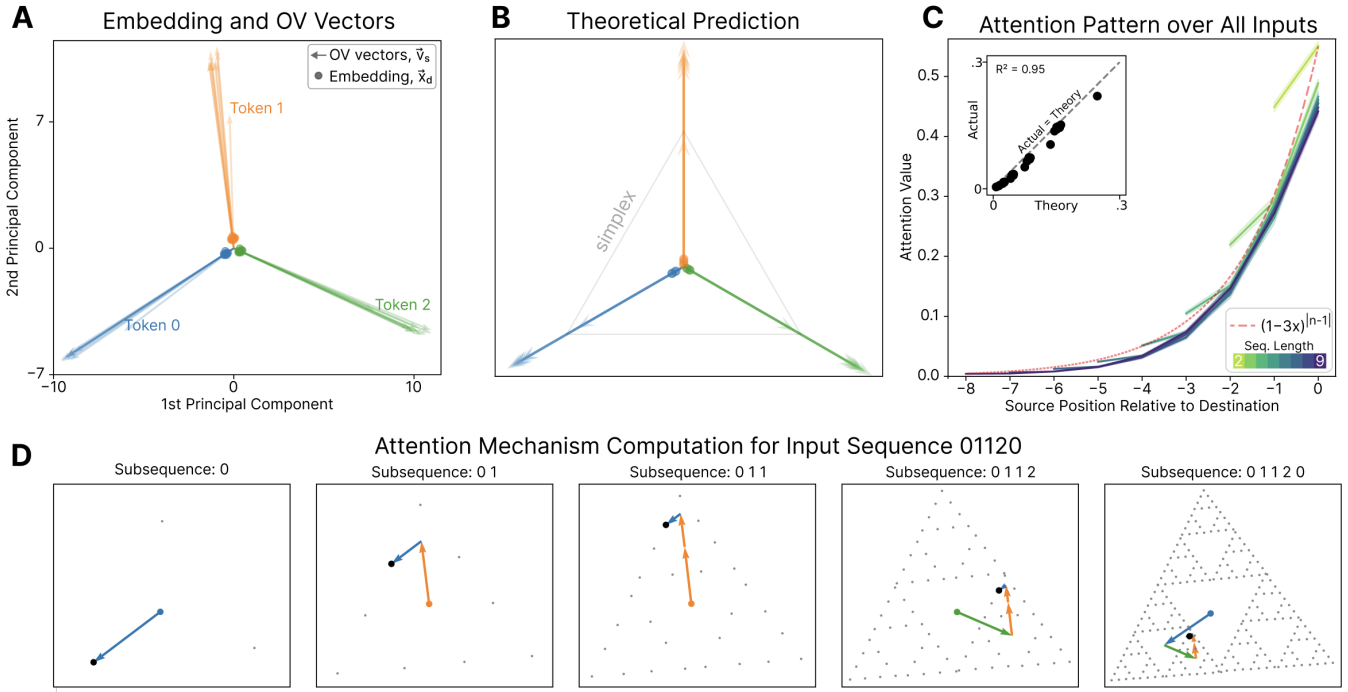**D** Attention Mechanism Computation for Input Sequence 01120

FIG. 2. **Intermediate Representation Construction by Attention.** A transformer trained on Mess3 with $x = 0.15$ and $\alpha = 0.6$ exhibits intermediate representations constructed through a specific attention mechanism. **(A)** The OV vectors (arrows) form three distinct clusters, each corresponding to a token and positioned at the vertices of a triangle, while token embeddings (circles) are clustered near the origin. **(B)** Our theoretical predictions for the OV vectors (shown for all (position, token) pairs) and embeddings (for positions > 2) align closely to those found in the trained transformer. **(C)** Attention patterns are primarily determined by the positional distance between the destination and source tokens, following an exponential decay described by $(1 - 3x)^{|n-1|}$. They are largely independent of specific token sequences. **(C, inset)** The theoretical (Eq. (13)) and actual values in the attention pattern align closely. **(D)** Construction of intermediate representations for five input subsequences of increasing length (from the example sequence 01120, shown left to right). The attention mechanism builds the fractal by taking linear combinations of the three $\vec{v}_s$ vectors. The colored vectors illustrate the components of the sum for each example subsequence, while the gray dots represent all possible vector sums for all sequences at that position.

source position s, d_h is the head dimension, and W_Q and W_K are each $d_h \times d_{model}$ weight matrices. Recall that attention is non-negative $0 \le A_{d,s} \le 1$ and, for each destination position d, the attention to all sources sums to one: $\sum_{s \le d} A_{d,s} = 1$. Eq. (3) shows how each attention head computes its update by weighting the transformed values ($\vec{v}_s$) from all previous positions according to their relevance ($A_{d,s}$) to the current position.

Our analysis yields several key insights into how the attention mechanism constructs the intermediate representations. First, we find that projecting token embeddings (the inputs into the attention head) onto PCA space reveals three clusters that lie close to the origin, as shown in Fig.2A. Meanwhile, the OV projections form update vectors $\vec{v}_s$ that cluster in three directions pointing toward the vertices of a triangle, naturally interpreted as the vertices of the belief simplex in Fig. 2. The model combines these directions through weights $A_{d,s}$ determined by the QK circuit as described by Eq. (3). For Mess3, these attention weights are nearly invariant to token identity

and decay exponentially with distance from the current position, controlling how past information is integrated. As the attention weight decays with distance, the impact of past tokens on the current belief state diminishes over time. Through this process of weighted vector addition within the belief simplex, the attention mechanism constructs the intermediate representations, resulting in the observed fractal structure shown in Figure 2D. Incredibly, *the computation the attention head performs is completely interpretable as a dynamic process in the belief simplex.*

C. Relating Intermediate Representations to Belief Updating Equations

The interpretation of attention as operating in the belief simplex suggests a connection to the theory of belief updating. Since the OV circuit is only able to access information from the source token that is attended to, we can write a constrained belief updating equation that sums

contributions from the value of the token $n = d - s$ places back for each value of n, assuming the initial belief is the stationary distribution of the HMM, $\boldsymbol{\pi}$. This gives the following equation for the constrained belief at position d in the sequence:

$$r_1^{(z_{1:d})} = \boldsymbol{\pi} + \sum_{s=1}^{d} \left(\boldsymbol{\pi} T^{|z_s} T^{d-s} - \boldsymbol{\pi} \right) \qquad (5)$$

where T is the HMM's hidden state transition matrix (marginalizing out the emissions), and $T^{|z}$ is the HMM transition matrix conditioned on seeing token z (see Appendix A for details).

Eq. (5), interpreted as a context-induced point in a vector space, is the natural geometric embedding of

$$\Pr(S_d) + \sum_{s=1}^{d} \left[\Pr(S_d|Z_s = z_s) - \Pr(S_d) \right] . \qquad (6)$$

This equation describes the best possible embedding if you haven't seen any context, $\Pr(S_d) = \boldsymbol{\pi}$, followed by independent corrections to that prediction from the token at each preceding context position, $\Pr(S_d|Z_s = z_s) - \Pr(S_d) = \boldsymbol{\pi} T^{|z_s} T^{d-s} - \boldsymbol{\pi}$. Notably, since Eq. (6) is a distribution over latent states S_d rather than merely the next token Z_{d+1}, this constrained updating equation naturally implemented by attention implies a probability density over all extended futures $Z_{d+1:}$ rather than just the next timestep.

Eq. (5)'s constrained belief geometry closely matches the intermediate structure observed in the central range of $\alpha \in [0.2, 0.6]$. As α moves further from this range, we observe gradually increasing deviations between predicted and actual representations, though the overall structure remains similar. A complete characterization of how these deviations scale with α remains for future work.

D. Attention Implements a Spectral Algorithm to Build the Constrained Beliefs

As seen in Eq. (5), the attention pattern in our model must relate to powers of the Markov transition matrix of the underlying hidden states, T^n, where n is the relative token distance.

When T is diagonalizable with a set of eigenvalues Λ_T, it then has a simple spectral decomposition such that we can rewrite Eq. (5) as

$$r_1^{(z_{1:d})} = \boldsymbol{\pi} + \sum_{s=1}^{d} \sum_{\lambda \in \Lambda_T \setminus \{1\}} \lambda^{d-s} \boldsymbol{\pi} T^{|z_s} T_\lambda \qquad (7)$$

where T_λ is the spectral projection operator associated with eigenvalue λ [16]. In this diagonalizable case, $T_\lambda = \sum_{k=1}^{a_\lambda} |\lambda_k\rangle\langle\lambda_k|$, where a_λ is the algebraic multiplicity of the eigenvalue λ, with right eigenstates satisfying $T|\lambda_k\rangle = \lambda|\lambda_k\rangle$, left eigenstates satisfying $\langle\lambda_k|T = \lambda\langle\lambda_k|$, all satisfying the orthonormality condition $\langle\lambda_j|\lambda_k\rangle = \delta_{j,k}$. Notably in Eq. (7), all dependence on inter-token distance now lies solely in the exponentiation of the eigenvalues, which all live on or within the unit circle in the complex plane for a stochastic transition matrix like T.

For the Mess3 process, the stochastic matrix T has eigenvalues $\Lambda_T = \{1, \zeta\}$, where $\zeta = 1 - 3x$ is a degenerate eigenvalue with multiplicity $a_\zeta = 2$. We observed that the attention weight n tokens back is approximately $\zeta^n = (1 - 3x)^n$, which suggests a strong connection between the theoretically motivated Eq. (7) and the architectural-implementation Eq. (3). Encouraged by this correspondence and further evidence of similarity, we make the ansatz that *the role of attention in the first layer is to implement the constrained belief update of Eq. (6) via Eq. (7)'s spectral mechanism.* [1] Taking this ansatz seriously allows us to precisely anticipate the analytic form of the learned attention pattern.

To derive the analytic form of the attention pattern, we assume that there is a linear map $f : \mathbb{R}^{d_{model}} \to \mathbb{R}^{|\mathcal{S}|-1}$ from the residual stream to the hyperplane containing the probability simplex over the hidden states of a minimal generative model of the data (the 2-simplex in this case). Let $\Pi_{\boldsymbol{\Delta}} = I - T_1 = I - \mathbf{1}\boldsymbol{\pi}$ be the projection from $\mathbb{R}^{|\mathcal{S}|}$ to the hyperplane $\mathbb{R}^{|\mathcal{S}|-1}$ containing the simplex. Our full ansatz is thus $f(\vec{x}_d^{(mid)}) = r_1^{(z_{1:d})} \Pi_{\boldsymbol{\Delta}}$ or, more explicitly:

$$f(\vec{x}_d^{(mid)}) = \sum_{s=1}^{d} \sum_{\lambda \in \Lambda_T \setminus \{1\}} \lambda^{d-s} \boldsymbol{\pi} T^{|z_s} T_\lambda \qquad (8)$$

$$= f(\vec{x}_d^{(pre)}) + \sum_{s \leq d} A_{d,s} f(\vec{v}_s) . \qquad (9)$$

From this, we group source-specific terms to infer that

$$f(\vec{x}_d^{(pre)}) + A_{d,d} f(\vec{v}_d) = \boldsymbol{\pi} T^{|z_d} - \boldsymbol{\pi} \qquad (10)$$

and

$$A_{d,s} f(\vec{v}_s) = \sum_{\lambda \in \Lambda_T \setminus \{1\}} \lambda^{d-s} \boldsymbol{\pi} T^{|z_s} T_\lambda \quad \text{for d} > \text{s} . \qquad (11)$$

From Eq. (11), we notice that $f(\vec{v}_s)$ is in the linear span of the non-stationary left eigenstates of T. I.e., $f(\vec{v}_s) \in$

---

[1] The details of this correspondence break down if there are many attention heads in the first layer.

$\mathrm{span}\big(\{\langle\lambda| : \lambda\,\langle\lambda| = T\,\langle\lambda| \text{ and } \lambda \neq 1\}\big)$ and, in particular, $f(\vec{v}_{\mathrm{s}}) \cdot |1\rangle = 0$ such that *adding any of the OV vectors to any stochastic vector (whose elements by definition add to one) keeps you in the hyperplane of the probability simplex.*

For the Mess3 family of processes, T has a single eigenvalue $\zeta = 1 - 3x$ with multiplicity $a_\zeta = 2$ besides its eigenvalue of 1. Accordingly, Eq. (11) simplifies to

$$A_{\mathrm{d,s}} f(\vec{v}_{\mathrm{s}}) = \zeta^{\mathrm{d-s}}\boldsymbol{\pi} T^{|z_{\mathrm{s}}} T_\zeta \qquad \text{for d > s }, \quad (12)$$

which forces $f(\vec{v}_{\mathrm{s}}) = c\boldsymbol{\pi} T^{|z_{\mathrm{s}}} T_\zeta$ for some $c \in \mathbb{R}$ independent of d, from which we obtain

$$A_{\mathrm{d+m,s}} = \zeta^m A_{\mathrm{d,s}} \qquad \text{for d > s }. \quad (13)$$

So, for example, $A_{2,1}$ implies $A_{\mathrm{d,1}}$ for all destinations d ≥ 2; and $A_{3,2}$ implies $A_{\mathrm{d,2}}$ for all destinations d ≥ 3.

For Mess3, $T_\zeta = I - |1\rangle\langle1| = I - \mathbf{1}\boldsymbol{\pi}$, since all projection operators must sum to the identity. Combining this insight with Eq. (12) tells us about the OV-vector for all positions:

$$f(\vec{v}_m) = \frac{\zeta}{A_{m+1,m}}\big(\boldsymbol{\pi} T^{|z_m} - \boldsymbol{\pi}\big) . \quad (14)$$

Notably, Eq. (14) tells us that all OV-vectors associated with the same token must be parallel—$f(\vec{v}_{\mathrm{s}}) \propto f(\vec{v}_{\mathrm{s'}})$ if $z_{\mathrm{s}} = z_{\mathrm{s'}}$—which is consistent with what we observe in our experiments (Fig. 2A). Moreover, the magnitude of the mth OV-vector is inversely proportional to the attention element $A_{m+1,m}$, which is again consistent with our experiments (Fig. 2AB). In our experiments, we find $A_{2,1}$ to be significantly larger than all the other $A_{m+1,m}$ elements, while the latter all cluster together; the magnitude of $\vec{v}_1$ is correspondingly smaller than all of the other strongly clustered $\vec{v}_m$ magnitudes.

Combining Eqs. (10) and (14) constrains the embedding

$$f(\vec{x}_m^{\,(\mathrm{pre})}) = \Big(1 - \frac{\zeta A_{m,m}}{A_{m+1,m}}\Big)\big(\boldsymbol{\pi} T^{|z_m} - \boldsymbol{\pi}\big) \quad (15)$$

to be parallel to the OV-vectors, as we indeed observe.

Eqs. (13), (14) and (15) make *strong predictions about the form of the attention pattern and how it relates to OV-vectors and token embeddings*, which must be true if the first layer of attention is indeed implementing the constrained belief updates over latent states of a generative model of the training data. These relationships are all borne out in our experiments (Fig. 2ABC), except for some scalar discrepancy in the first two embedding vectors (see Appendix C for quantification), which is a strong validation of the predictive power of our framework.

1. Negative eigenvalues require more attention heads

For the transition matrix T to be row stochastic (a requirement for a valid HMM), x must be in the range $[0, 1/2]$. Interestingly, when $\zeta < 0$ (which occurs when $x > 1/3$), the predicted pattern oscillates and cannot be captured by a single attention head, since attention pattern entries must be non-negative. In these cases, we observe that a single-head transformer captures an incomplete representation of the belief state geometry, and the transformer performs correspondingly worse (Appendix D). However, upon adding a second attention head, the model converges to the solution predicted by the belief updating equation, even in the presence of oscillatory dynamics, as shown in Fig. 3.

The anticipated need for a second attention head when the data-generating transition matrix has a negative eigenvalue further demonstrates how our analysis provides a handle to relate the architectural constraints of the attention mechanism to the structure of the training data. In fact, our framework provides more specific predictions for the attention pattern and its relation to embedding and OV-vectors in this case too.

With two attention heads, the update to the residual stream at the destination position d becomes

$$\vec{c}_{\mathrm{d}} = \sum_{\mathrm{s}=1}^{\mathrm{d}} \sum_{h=1}^{2} A_{\mathrm{d,s}}^{(h)} \vec{v}_{\mathrm{s}}^{\,(h)} , \quad (16)$$

where each head now has its own QK and OV matrices. With the negative eigenvalue $\zeta < 0$ and two attention
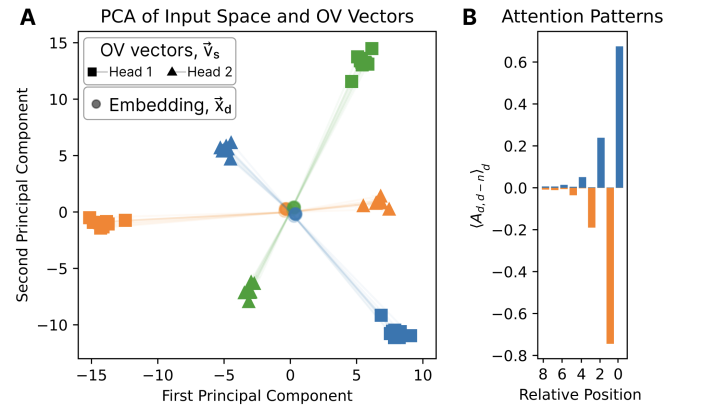

FIG. 3. Attention heads combine to capture oscillatory dynamics in belief updating. (a) In the token embedding space, the model uses each attention head to embed tokens on opposite poles of the simplex. (b) The attention patterns of the two heads (shown here averaged over all sequences) act as positive and negative components. When combined, they produce the oscillatory pattern predicted by the exponentiated eigenvalue $\zeta^n = (-1)^n (3x - 1)^n \propto A_{\mathrm{s+n,s}}^{(1)} |f(\vec{v}_{\mathrm{s}}^{(1)})| - A_{\mathrm{s+n,s}}^{(2)} |f(\vec{v}_{\mathrm{s}}^{(2)})|$.

heads, we can relate the constrained belief update to the details of attention and embedding via

$$f(\vec{x}_{\text{d}}^{\,(\text{mid})}) = \sum_{\text{s}=1}^{\text{d}} (-1)^{\text{d}-\text{s}}(-\zeta)^{\text{d}-\text{s}}\boldsymbol{\pi}T^{|z_{\text{s}}}T_{\zeta} \qquad (17)$$

$$= f(\vec{x}_{\text{d}}^{\,(\text{pre})}) + \sum_{\text{s}\leq\text{d}} \left[A_{\text{d,s}}^{(1)}f(\vec{v}_{\text{s}}^{(1)}) + A_{\text{d,s}}^{(2)}f(\vec{v}_{\text{s}}^{(2)}) \right] .$$

This is naturally accommodated by

$$A_{\text{d,s}}^{(1)}f(\vec{v}_{\text{s}}^{(1)}) = +\delta_{+1,(-1)^{\text{d}-\text{s}}}|\zeta|^{\text{d}-\text{s}}\boldsymbol{\pi}T^{|z_{\text{s}}}T_{\zeta} \quad \text{and} \quad (18)$$

$$A_{\text{d,s}}^{(2)}f(\vec{v}_{\text{s}}^{(2)}) = -\delta_{-1,(-1)^{\text{d}-\text{s}}}|\zeta|^{\text{d}-\text{s}}\boldsymbol{\pi}T^{|z_{\text{s}}}T_{\zeta} \qquad (19)$$

for $\text{d} > \text{s}$, which implies that the OV-vectors point in opposite directions, $\widehat{f(\vec{v}_{\text{s}}^{(1)})} = -\widehat{f(\vec{v}_{\text{s}}^{(2)})}$, with $f(\vec{v}_{\text{s}}^{(h)}) \propto (\boldsymbol{\pi}T^{|z_{\text{s}}} - \boldsymbol{\pi})$ and

$$A_{\text{d}+2m,\text{s}}^{(h)} = \zeta^{2m} A_{\text{d,s}}^{(h)} \qquad \text{for d} > \text{s} , \qquad (20)$$

consistent with our experiments as shown in Fig. 3. We note that the magnitudes of OV vectors are tied to attention magnitudes via $c\zeta^{\text{d}-\text{s}} = A_{\text{d,s}}^{(1)}|f(\vec{v}_{\text{s}}^{(1)})| - A_{\text{d,s}}^{(2)}|f(\vec{v}_{\text{s}}^{(2)})|$, with $c = |\boldsymbol{\pi}T^{|z_{\text{s}}} - \boldsymbol{\pi}| \in \mathbb{R}$, which is also observed in Fig. 3.

E. Post-MLP geometries

While the intermediate geometry is well characterized by our constrained belief equations, the transformation performed by the MLP is more complex. Through purely local computations at each position, the MLP learns a continuous nonlinear warping that transforms the intermediate fractal structure into the final belief geometry.

Figure 4 provides a comprehensive comparison between theoretical predictions and observed representations across different parameter settings of the Mess3 HMM. The close match between predicted and actual geometries, both for intermediate and final representations, confirms our theoretical understanding of the transformer's computational process. The transformation between these geometries involves stretching and compressing different regions of the space, maintaining the topological structure while aligning it with theoretically optimal belief representations.

The remarkable precision and consistency of this learned transformation raises intriguing questions about the nature of this mapping. While we observe that distinct regions remain well-separated through the transformation, a full characterization of its mathematical properties remains an exciting direction for future work.
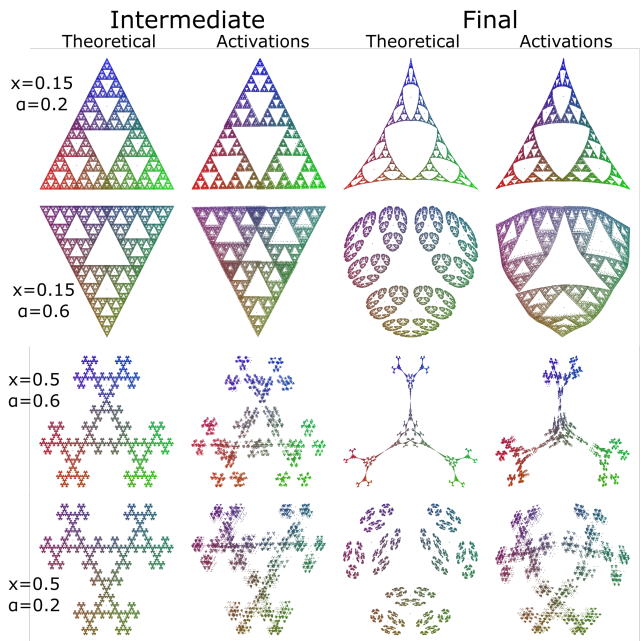

FIG. 4. Comparison of model representations and theoretical predictions for different Mess3 hyperparameters in each row. Each subfigure shows four columns: (i) Intermediate representation from Eq. (5). (ii) PCA projection of the model activations in the intermediate layer. (iii) Ground truth belief state geometry from Eq. (2). (iv) PCA projection of the final activations after the MLP.

V. DISCUSSION AND CONCLUSION

We have shown how combining **computational mechanics** with **mechanistic interpretability** yields a principled understanding of why transformers trained on Mess3 HMM data learn intermediate fractal-like structures, and how these structures systematically transition into final belief-state representations. Our analysis provides a top-down theoretical explanation grounded in the tension between optimal Bayesian belief updates and the parallel, attention-based constraints of transformer computation, developing geometric observations of activation space into mechanistic understanding of the underlying computational principles.

Implications for interpretability. — Our work demonstrates an alternative to purely bottom-up architectural analysis. Knowing the structure of optimal predictors allows us to predict—and ultimately verify—the *specific* intermediate computations that are implemented under the attention mechanism. Our analysis reveals the computational role of specific directions in activation space—showing how the geometry of belief updates shapes the learned representations. Additionally, by focusing on a small, tractable HMM, we see how specific properties of its transition matrix lead to oscillatory patterns that require

specialized multi-head solutions due to the non-negativity constraints of attention mechanisms. Rather than relying on general observations that attention heads specialize, our analysis reveals precisely *why* and *how* multiple heads must coordinate: the non-negativity constraints of attention, combined with oscillatory patterns in optimal belief updates, necessitate specific decompositions across heads, providing concrete mechanistic understanding of their functional roles. This demonstrates how combining theoretical understanding with architectural constraints can yield precise, verifiable interpretations of neural network components.

Limitations and future work. — We focused on small transformers and the specialized Mess3 family of HMMs with full support over the space of all possible sequences of tokens. We discovered how transformers implement belief updates when attention patterns depend primarily on positional distances, while token-specific information is handled through value vectors. Our techniques must be adapted to both more general transformer architectures and data-generating processes that capture the complexities of real-world data. While this setting offers clear insights, it does not capture many aspects of natural language. Future work could apply these techniques to processes that better reflect properties of natural language—hierarchical, with sparse support over sequences—and to transformers at larger scales. Moreover, the interplay between multi-head attention and deeper layer stacks likely exhibits additional nuances that our single-layer analyses only begin to uncover. Finally, while we showed that the final MLP layer refines partial updates to approximate full Bayes, the deeper question of why gradient descent converges on these circuits remains ripe for further investigation.

Conclusion. — By combining computational mechanics with mechanistic interpretability, we have shown how transformers implement inherently recursive Bayesian updates through parallel computations via the attention mechanism, and how these intermediate representations are refined into the final form. This reconciles model-agnostic theories of next-token prediction with the reality of architecture-specific constraints. We hope our results not only advance interpretability for HMM-like toy tasks but also inspire deeper theoretical insights into how large-scale transformers produce—and exploit—belief-like structures in real-world applications.

Author Contributions

MP discovered the attention-based constrained belief updating algorithm in the simplex, and performed the bulk of the experiments with mentorship from ASS. PMR developed the mathematical theory together with MP and ASS. ASS supervised the project, and DF provided project management. MP, PMR, and ASS wrote the manuscript, with helpful guidance from DF. MP, PMR, and ASS performed analysis, and established the correspondence between transformer behavior and theoretical predictions.

[1] Bricken, T., Templeton, A., Batson, J., Chen, B., Jermyn, A., Conerly, T., Turner, N., Anil, C., Denison, C., Askell, A., Lasenby, R., Wu, Y., Kravec, S., Schiefer, N., Maxwell, T., Joseph, N., Hatfield-Dodds, Z., Tamkin, A., Nguyen, K., McLean, B., Burke, J. E., Hume, T., Carter, S., Henighan, T., and Olah, C. Towards monosemanticity: Decomposing language models with dictionary learning. *Transformer Circuits Thread*, 2023. URL https://transformer-circuits.pub/2023/monosemantic-features/index.html. 2

[2] Conmy, A., Mavor-Parker, A. N., Lynch, A., Heimersheim, S., and Garriga-Alonso, A. Towards automated circuit discovery for mechanistic interpretability, 2023. URL https://arxiv.org/abs/2304.14997. 2

[3] Crutchfield, J. P. The calculi of emergence: Computation, dynamics, and induction. *Physica D*, 75:11–54, 1994. 3

[4] Crutchfield, J. P. Between order and chaos. *Nature Physics*, 8(1):17–24, 2012. 3

[5] Cunningham, H., Ewart, A., Riggs, L., Huben, R., and Sharkey, L. Sparse autoencoders find highly interpretable features in language models, 2023. URL https://arxiv.org/abs/2309.08600. 2

[6] Elhage, N., Nanda, N., Olsson, C., Henighan, T., Joseph, N., Mann, B., Askell, A., Bai, Y., Chen, A., Conerly, T., DasSarma, N., Drain, D., Ganguli, D., Hatfield-Dodds, Z., Hernandez, D., Jones, A., Kernion, J., Lovitt, L., Ndousse, K., Amodei, D., Brown, T., Clark, J., Kaplan, J., McCandlish, S., and Olah, C. A mathematical framework for transformer circuits. *Transformer Circuits*

Thread, 2021. URL https://transformer-circuits.pub/2021/framework/index.html. 1, 2, 4

[7] Elhage, N., Hume, T., Olsson, C., Schiefer, N., Henighan, T., Kravec, S., Hatfield-Dodds, Z., Lasenby, R., Drain, D., Chen, C., Grosse, R., McCandlish, S., Kaplan, J., Amodei, D., Wattenberg, M., and Olah, C. Toy models of superposition. *Transformer Circuits Thread*, 2022. URL https://transformer-circuits.pub/2022/toy_model/index.html. 2

[8] Engels, J., Michaud, E. J., Liao, I., Gurnee, W., and Tegmark, M. Not all language model features are linear. *arXiv preprint arXiv:2405.14860*, 2024. 2

[9] Kaelbling, L. P., Littman, M. L., and Cassandra, A. R. Planning and acting in partially observable stochastic domains. *Artificial intelligence*, 101(1-2):99–134, 1998. 3

[10] Kingma, D. P. and Ba, J. Adam: A method for stochastic optimization, 2017. URL https://arxiv.org/abs/1412.6980. 12

[11] Marks, S., Rager, C., Michaud, E. J., Belinkov, Y., Bau, D., and Mueller, A. Sparse feature circuits: Discovering and editing interpretable causal graphs in language models, 2024. URL https://arxiv.org/abs/2403.19647. 2

[12] Marzen, S. E. and Crutchfield, J. P. Nearly maximally predictive features and their dimensions. *Physical Review E*, 95(5), May 2017. ISSN 2470-0053. doi: 10.1103/physreve.95.051301. URL http://dx.doi.org/10.1103/PhysRevE.95.051301. 1, 3

[13] Nanda, N., Chan, L., Lieberum, T., Smith, J., and Steinhardt, J. Progress measures for grokking via mechanistic interpretability, 2023. URL https://arxiv.org/abs/2301.05217. 1, 2

[14] Park, K., Choe, Y. J., and Veitch, V. The linear representation hypothesis and the geometry of large language models, 2024. URL https://arxiv.org/abs/2311.03658. 2

[15] Pepper, K. RNNs represent belief state geometry in their hidden states. https://apartresearch.com, June 2024. Research submission to the Computational Mechanics Hackathon research sprint co-hosted by Apart, PIBBSS, and Simplex. 1, 3

[16] Riechers, P. M. and Crutchfield, J. P. Beyond the spectral theorem: Decomposing arbitrary functions of nondiagonalizable operators. *AIP Advances*, 8:065305, 2018. 6

[17] Riechers, P. M. and Crutchfield, J. P. Spectral simplicity of apparent complexity, Part I: The nondiagonalizable metadynamics of prediction. *Chaos*, 28:033115, 2018. doi:10.1063/1.4985199. 1, 3

[18] Shai, A. S., Marzen, S. E., Teixeira, L., Oldenziel, A. G., and Riechers, P. M. Transformers represent belief state geometry in their residual stream. *accepted to Advances in Neural Information Processing Systems 37 (NeurIPS 2024)*, 2024. URL https://arxiv.org/abs/2405.15943. 3

[19] Shalizi, C. R. and Crutchfield, J. P. Computational mechanics: Pattern and prediction, structure and simplicity. *Journal of statistical physics*, 104:817–879, 2001. 1, 3

[20] Templeton, A., Conerly, T., Marcus, J., Lindsey, J., Bricken, T., Chen, B., Pearce, A., Citro, C., Ameisen, E., Jones, A., Cunningham, H., Turner, N. L., McDougall, C., MacDiarmid, M., Freeman, C. D., Sumers, T. R., Rees, E., Batson, J., Jermyn, A., Carter, S., Olah, C.,

and Henighan, T. Scaling monosemanticity: Extracting interpretable features from claude 3 sonnet. *Transformer Circuits Thread*, 2024. URL https://transformer-circuits.pub/2024/scaling-monosemanticity/index.html. 2

[21] Upper, D. R. *Theory and algorithms for hidden Markov models and generalized hidden Markov models.* University of California, Berkeley, 1997. 3

[22] Vaswani, A., Shazeer, N., Parmar, N., Uszkoreit, J., Jones, L., Gomez, A., Kaiser, L., and Polosukhin, I. Attention is all you need. *Advances in Neural Information Processing Systems*, 2017. 1, 4

[23] Wang, K., Variengien, A., Conmy, A., Shlegeris, B., and Steinhardt, J. Interpretability in the wild: a circuit for indirect object identification in gpt-2 small, 2022. URL https://arxiv.org/abs/2211.00593. 2

Appendix A: Mathematical Details of HMMs and Belief State Geometry

In this work we created training data from a class of Hidden Markov Models (HMMs) called Mess3. The HMMs have three hidden states $\mathcal{S} = \{1, 2, 3\}$ and emit from a vocabulary of three tokens $\mathcal{Z} = \{0, 1, 2\}$.

The HMMs in this class are parameterized by α and x, with dependent quantities $\beta = (1 - \alpha)/2$ and $y = 1 - 2x$.

The labeled transition matrices define the probability of moving to state j (indexing columns) and emitting the token on the label, z, conditioned on being in state i (indexing rows), $P(s_j, z|s_i)$ and are:

$$T^{(0)} = \begin{bmatrix} \alpha y & \beta x & \beta x \\ \alpha x & \beta y & \beta x \\ \alpha x & \beta x & \beta y \end{bmatrix} \tag{A1}$$

$$T^{(1)} = \begin{bmatrix} \beta y & \alpha x & \beta x \\ \beta x & \alpha y & \beta x \\ \beta x & \alpha x & \beta y \end{bmatrix} \tag{A2}$$

$$T^{(2)} = \begin{bmatrix} \beta y & \beta x & \alpha x \\ \beta x & \beta y & \alpha x \\ \beta x & \beta x & \alpha y \end{bmatrix} \tag{A3}$$

Note that even though the dynamics amongst the emissions are infinite-Markov order, the dynamics amongst the hidden states are Markov, with a transition matrix given by marginalizing out the token emissions: $T = \sum_{z \in \mathcal{Z}} T^{(z)}$.

Since Mess3 has non-zero row sums for each labeled transition matrix, we can also define a conditional transition matrix, $T^{|z}$, with elements $T^{|z}_{i,j} = \Pr(s_j|z, s_i) = \Pr(s_j, z|s_i)/\Pr(z|s_i) = T^{(z)}_{i,j}/(\sum_j T^{(z)}_{i,j})$, which is given by normalizing each labeled transition matrix such that every row sums to 1.

1. Full belief updates

An important part of the work presented here is about how an optimal observer of token emissions from the HMM would update their beliefs over which of the hidden states the HMM is in, given a token sequence. If the observer is in a belief state given by a probability distribution $\boldsymbol{\eta}$ (a row vector) over the hidden states of the data-generating process, then the update rule for the new belief state $\boldsymbol{\eta}'$ given that the observer sees a new token z is:

$$\boldsymbol{\eta}' = \frac{\boldsymbol{\eta} T^{(z)}}{\boldsymbol{\eta} T^{(z)} \mathbf{1}} \tag{A4}$$

where $\mathbf{1}$ is a column vector of ones of appropriate dimension, with the denominator ensuring proper normalization of the updated belief state. In general, starting from the initial belief state $\boldsymbol{\eta}_\varnothing$, we can find the belief state after observing a sequence of tokens $z_0, z_1, \ldots, z_N$:

$$\vec{r}^{(z_{1:d})}_{\text{full}} = \frac{\boldsymbol{\eta}_\varnothing T^{(z_0)} T^{(z_1)} \cdots T^{(z_N)}}{\boldsymbol{\eta}_\varnothing T^{(z_0)} T^{(z_1)} \cdots T^{(z_N)} \mathbf{1}} \ . \tag{A5}$$

For stationary processes, the optimal initial belief state is given by the stationary distribution $\boldsymbol{\eta}_\varnothing = \boldsymbol{\pi}$ over hidden states of the HMM (the left-eigenvector of the transition matrix $T = \sum_z T^{(z)}$ associated with the eigenvalue of 1).

The beliefs have a geometry associated with them, called the belief-state geometry. The belief-state geometry is given by plotting the belief distribution over the HMM's hidden states induced from each possible sequence of tokens as a point in the probability simplex over these hidden states.

2.   Constrained belief updates

Incorporating past contributions to belief updates in parallel, as the attention mechanism suggests, we instead obtain

$$\vec{r}_1^{(z_{1:\mathrm{d}})} = \boldsymbol{\pi} + \sum_{n=0}^{\mathrm{d}-1} \left(\frac{\boldsymbol{\pi} T^{(z_{\mathrm{d}-n})} T^n}{\boldsymbol{\pi} T^{(z_{\mathrm{d}-n})} \mathbf{1}} - \boldsymbol{\pi} \right) \tag{A6}$$

For processes like Mess3 that have non-zero row sums for each labeled transition matrix, this can be written more simply as:

$$\vec{r}_1^{(z_{1:\mathrm{d}})} = \boldsymbol{\pi} + \sum_{n=0}^{\mathrm{d}-1} \left(\boldsymbol{\pi} T^{|z_{\mathrm{d}-n}} T^n - \boldsymbol{\pi} \right) , \tag{A7}$$

which is the form that appears in the main text. For other processes that don't satisfy this condition, slight modifications of the equations in the main text follow straightforwardly from Eq. (A6).

Appendix B: Model architecture and training procedure

We employ a standard single-layer transformer model with learned positional embeddings. The model architecture follows the conventional transformer design, with $d_{\mathrm{model}} = 64$ and $d_{\mathrm{ff}} = 256$. Depending on the Mess3 parameters, we use either a single-head or a double-head attention mechanism. We conduct a systematic sweep over the HMM parameters α and x, training a separate model for each pair. Models are trained on next-token prediction using cross-entropy loss, with batch size 128. We use Adam optimizer [10] with a 10^{-4} learning rate and no weight decay. Each model is trained for approximately 15 million tokens.

We generate all possible input sequences up to length 10, recording hidden activations from the transformer's residual stream. These activations are organized into a dataset capturing the model's response to all input patterns.

Input sequences consist of three symbols, embedded with positional information, without a beginning-of-sequence (BOS) token.

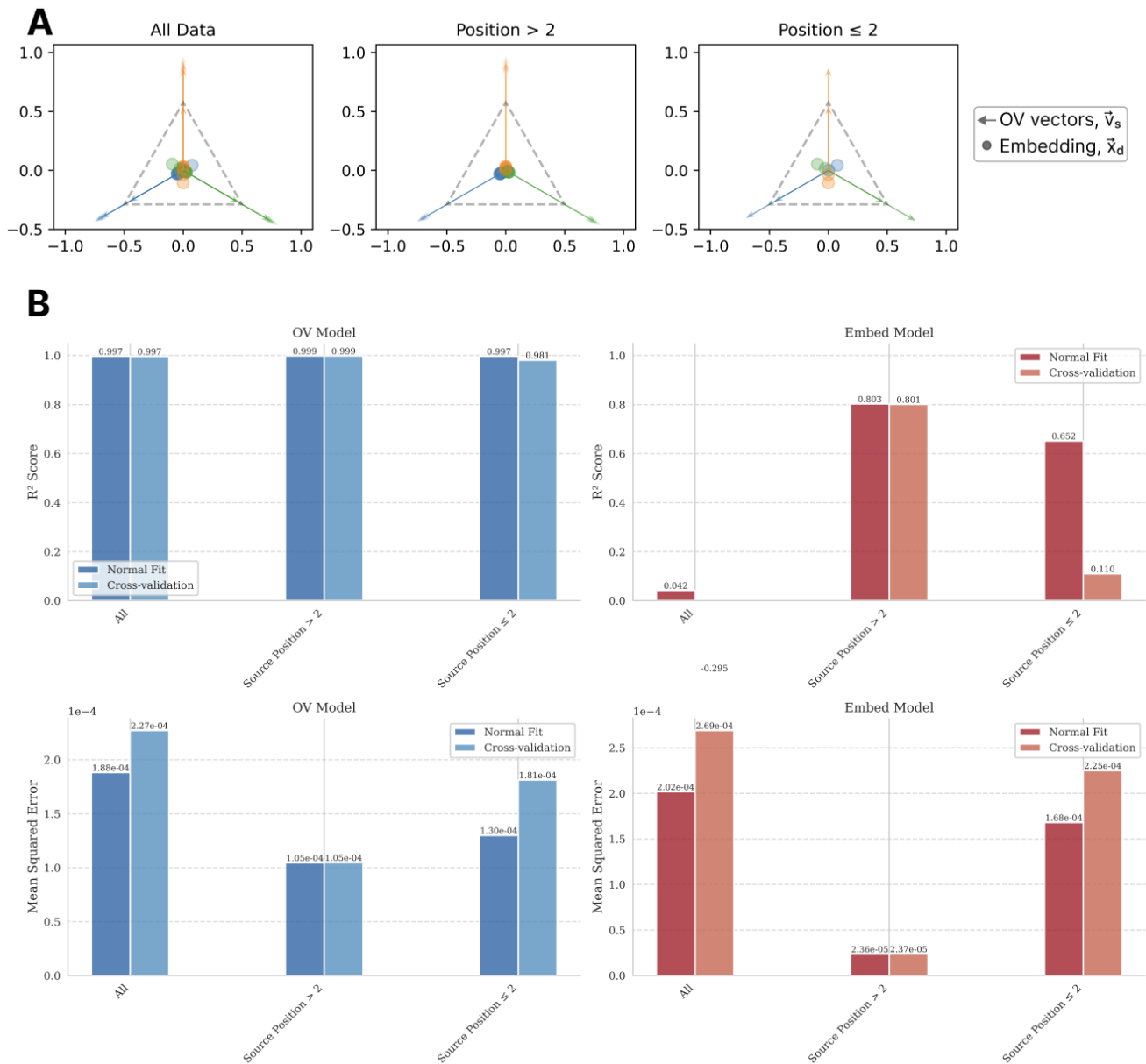## Appendix C: Quantification of Theoretical Predictions

FIG. 5. Embeddings for the first two positions are correctly predicted to be parallel to the OV vectors, as with all of the embeddings; however the sign of the predicted embedding for these first two positions deviates from the observed embedding. We do not yet understand the reason for this discrepancy, but still find it remarkable that the bulk of the high-dimensional computation carried out by attention—attention pattern, OV vectors, and all embeddings beyond the first two positions—can be very precisely understood by a sequence of operations in the two-dimensional simplex.

Appendix D: Minimal architectural requirements

To verify our theoretical understanding of the transformer's computational requirements, we conduct a systematic evaluation across different architectural configurations. Figure 6 shows that the model achieves good performance with minimal architecture: a single layer with two attention heads is sufficient to achieve low KL divergence across different
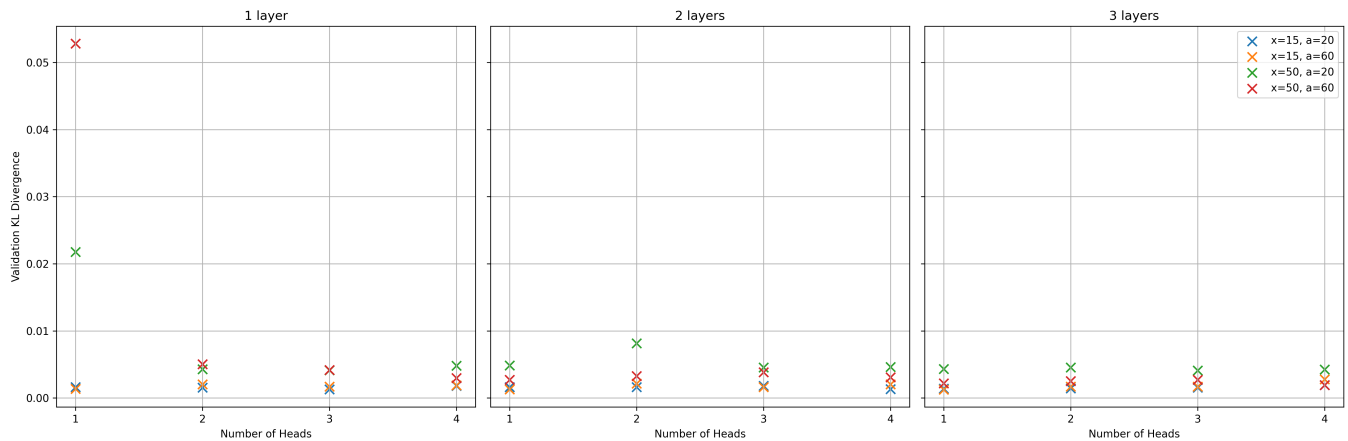
FIG. 6. Validation KL divergence between model predictions and optimal probabilities across different architectural configurations. Results shown for various Mess3 parameter settings (x and α) and model architectures (number of heads and layers). The model achieves good performance with minimal architecture: a single layer with two attention heads is sufficient across parameter settings.
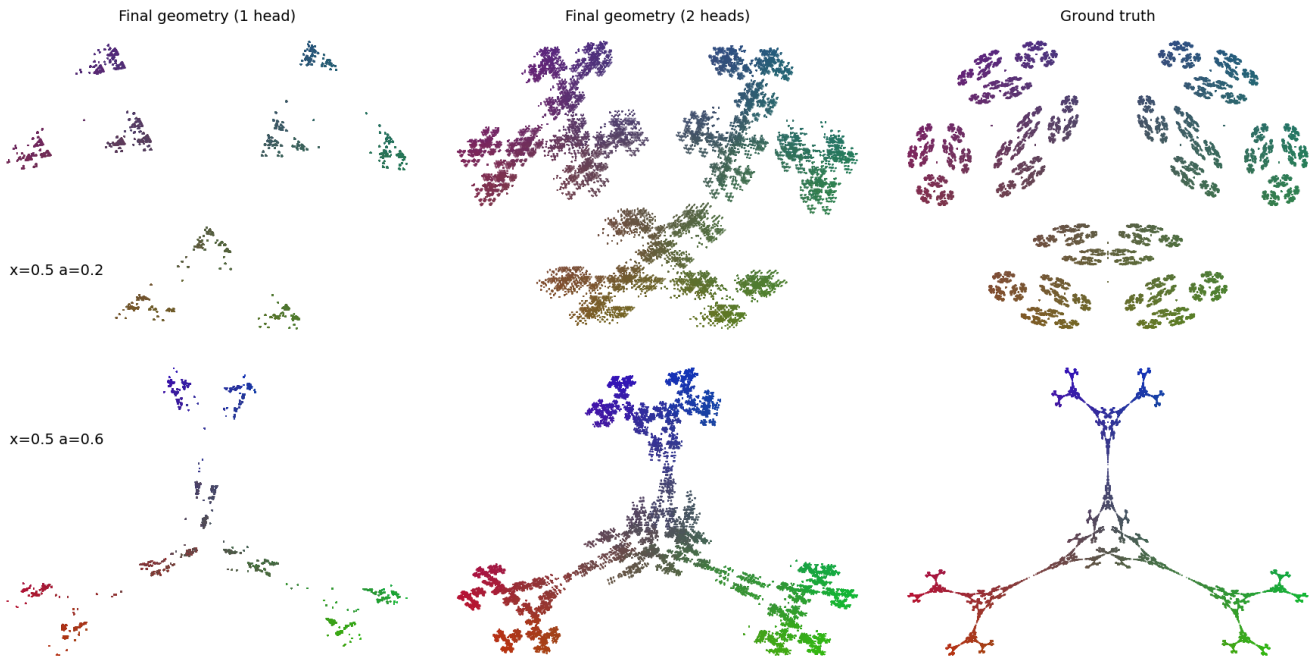

FIG. 7. Comparison of learned belief geometry with one head (left) versus two heads (middle) against ground truth (right) for two different Mess3 parameter settings. With $x = 0.5$, where the optimal update pattern requires both positive and negative components, a single head fails to capture the correct geometry due to the non-negativity constraint of attention. Two heads allow the model to properly implement these updates, resulting in geometry that closely matches the ground truth.

Mess3 parameter settings. This empirical finding aligns with our theoretical analysis: when $x > 1/3$, the belief update patterns contain oscillatory components that require two heads to implement due to the non-negativity constraint of attention. The necessity of two heads is visually demonstrated in Figure 7. For $x = 0.5$, where the optimal update pattern has significant oscillatory components, a single-head transformer fails to capture the correct belief geometry. With two heads, the model can properly implement these updates through complementary attention patterns, resulting in representations that closely match the ground truth geometry.

Appendix E: Dimensionality of Residual Stream Activations

TABLE I. Cumulative explained variance ratios for PCA components of the residual stream activations at the intermediate position (after attention) and the final position (before unembedding). The table shows results for different settings of the Mess3 HMM parameters x and α.

		Intermediate				Final			
	x	0.15	0.15	0.5	0.5	0.15	0.15	0.5	0.5
component	α	0.2	0.6	0.6	0.2	0.2	0.6	0.6	0.2
0		0.5408	0.4648	0.4074	0.5268	0.9618	0.4947	0.4596	0.6503
1		0.8768	0.8894	0.8028	0.8519	0.9825	0.7681	0.7096	0.8592
2		0.9673	0.9859	0.8913	0.9173	0.9943	0.9811	0.8855	0.9689
3		0.9749	0.9903	0.9455	0.9649	0.9960	0.9897	0.9189	0.9755
4		0.9815	0.9929	0.9848	0.9886	0.9969	0.9916	0.9428	0.9807
5		0.9870	0.9942	0.9978	0.9977	0.9976	0.9931	0.9586	0.9850
6		0.9914	0.9955	0.9986	0.9984	0.9981	0.9945	0.9723	0.9886

We perform PCA on the residual stream activations after the attention module (intermediate) and before the unembedding layer (final). The effective dimensionality of the residual stream is low, with the first few components capturing most of the variance (See Table I). In most cases, the first 3 components explain over 90% of the variance. For $x = 0.5$, the effective dimensionality is higher, possibly due to the oscillatory dynamics of the belief updating equation in this regime. Further investigation is needed to fully understand this phenomenon.